

Preparation and characterisation of calcium citrate wires

Liangzhao Zhong¹, Junfeng Li¹, Yang Gao¹, Wenqiang Cao¹, Peicong Zhang¹, Xuefei Lai²

¹Department of Materials Science and Engineering, Chengdu University of Technology, Chengdu 610059, People's Republic of China

²College of Chemical Engineering, Sichuan University, P.O. Box 610064, People's Republic of China
E-mail: lijunfeng@cdu.cn

Published in Micro & Nano Letters; Received on 8th March 2015; Revised on 20th May 2015; Accepted on 4th June 2015

Long calcium citrate wires were successfully prepared using a convenient and effective soft chemical method that involved heating the sheet precursor at an appropriate temperature in a mixture of alcohol and water for a sufficient amount of time. The X-ray diffraction patterns showed that the crystallinity degree increased with heating time. Moreover, the (200) crystal plane was the preferential growth face that was influenced by alcohol. Such influence was ascribed to alcohol being able to change the free energy and the supersaturation state of the solution. In addition, alcohol might adsorb onto the surface of the crystal and change the growth velocity of each crystal plane. The sheet precursor progressively turned into consecutive long wires by growing along the preferential growth orientation during the dissolution–reprecipitation process. The thickness of the wires was ~8–30 nm. Long calcium citrate wires were produced to reinforce and strengthen biomaterials or for other purposes.

1. Introduction: Calcium citrate has been used as a calcium supplement during the growing years of teenagers and to provide sufficient calcium to the elderly for osteoporosis prevention. In recent years, nanomaterials have been widely used in biomaterials; for example, the nano-calcium citrate group exhibited better effect than the micro group in the ICR mice test regarding serum calcium concentrations and bone mineral density [1]. This previous study also significantly demonstrated that calcium citrate was more effective than calcium carbonate.

Furthermore, calcium citrate has been studied as a new type of bone repair material because of its biocompatibility and high concentrations of calcium ions. Calcium citrate can positively stimulate fracture healing in Japanese white rabbits during the early time point when defects are not yet too large because calcium citrate may resorb faster than the calcium phosphate, hydroxyapatite [2]. Calcium citrate combined with recombinant human bone morphogenetic-2 (rhBMP-2) obviously enhances bone regeneration in bone defects [3]. As an organic acid salt, calcium citrate faces the problem of fast decomposition and low strength when it is used in bone repair. The degradation rate and mechanical property are significantly correlated with the structure and morphology. One of the most successful approaches to strengthen brittle materials and improve their strength is fibre reinforcement. The introduction of high-modulus fibre reinforcements has been reported; however, such studies tend to use conventional candidate fibres, such as carbon and glass fibres, which are durable *in vivo* [4].

Apart from fibres and wires, different morphologies and characteristics of calcium citrate have been generated for various properties. Calcium citrate has always been produced using citric acid and CaCO₃ or CaO because of their low cost; moreover, morphology is frequently neglected. Xing [5] chose oyster shell in his study to maintain the biological structure. Nano-calcium citrate was nanoscaled using a pulsed airflow pulveriser [1]. Herdtweck *et al.* [6] obtained needle-shaped crystals of [Ca₃(C₆H₅O₇)₂(H₂O)₂]·2H₂O through hydrothermal synthesis, which was a tool for improving the performance of calcium citrate using a soft chemical method. This approach can produce various morphologies, particularly fibres or wires.

2. Experimental

2.1. Materials: Calcium chloride anhydrous (CaCl₂, AR, 95%), trisodium citrate (Na₃C₆H₅O₇, AR, 99%) and ethyl alcohol (CH₃CH₂OH, AR, 95%) were purchased from the ChengDu KeLong Chemical Co. Ltd, China.

2.2. Preparing calcium citrate: Sodium citrate solution (0.12 mol/l) and calcium chloride solution (0.18 mol/l) were mixed. The mole ratio of calcium chloride/sodium citrate (CaCl₂/Na₃C₆H₅O₇) was exactly 3:2. Two kinds of solutions were mixed at 25°C. Then, the precursor (i.e. calcium citrate) precipitated when alcohol was added into the mixed solutions.

The precursor (~0.342 g) was poured into a beaker with water or an alcohol–distilled water mixture (160 ml H₂O, 80 ml CH₃CH₂OH) after filtration and cleaning. The volume ratio of alcohol/distilled water (CH₃CH₂OH/H₂O) was between 1:5 and 2:1, which could also be pure water. Lastly, calcium citrate wires were obtained after the mixture was maintained at 70–90°C for 2–10 h.

2.3. Characterisation: X-ray diffraction (XRD) analysis was performed using a DX-2700X diffractometer with Cu-K α radiation (Dandong Fangyuan Instrument Co. Ltd, China). The microstructures of the samples were investigated using a scanning electron microscope (SEM; JMS-5900lv, Hitachi Ltd, Japan). The infrared (IR) spectrum was obtained using a Fourier IR spectrometer (Tensor 27, Bruker Corporation, Germany). Raman spectra were obtained using an inVia confocal Raman microscope (Renishaw plc, UK) with a 514.5 nm laser. Thermoanalysis was performed with an STA 409 PC/PG device (Netzsch Group, Germany).

3. Results and discussion: The XRD patterns of the precursor are shown in Fig. 1, pattern *a*. In particular, Fig. 1, patterns *b–e* show the XRD patterns of the precursor that has undergone heating in an alcohol–water mixture for 2, 4, 6 and 8 h, respectively, at the same temperature. As shown in Fig. 1, the XRD patterns of the samples agree well with JCPDS No. 28-2003 [Ca₃(C₆H₅O₇)₂·4H₂O]. The precursor that was precipitated using alcohol was calcium citrate (Fig. 1, pattern *a*). The peaks of the (200), (400), (600) and (800) crystal planes were weak in Fig. 1, pattern *a*, and their strength increased as heating time lengthened (Fig. 1, patterns *b–e*). However, the opposite results were obtained in (–201) and (–112). The increase and decrease of the peaks revealed a preferential growth orientation under heating. The peak of the (200) crystal plane at $2\theta = 5.697^\circ$ was particularly obvious, and this plane would be one of the preferentially growing crystal faces. Among the preferentially growing directions was the means of calcium citrate morphology, such as a needle or wire. The peak height of the (200) plane increased, and the full width at

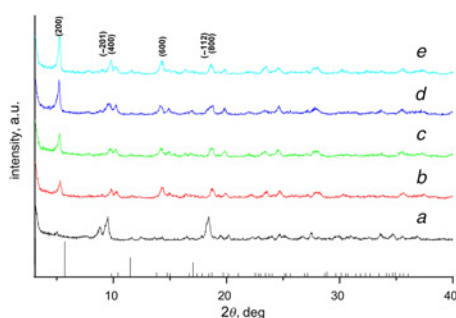


Figure 1 XRD patterns of calcium citrate that underwent heating at different times
a 0 h, b 2 h, c 4 h, d 6 h, e 8 h

half maximum narrowed down from patterns *a* to *e* in Fig. 1, which indicated that the crystallinity degree increased with heating time.

In the Fourier transform IR spectroscopy (FTIR) curve (see Fig. 2), the absorption bands located at 3477.6 and 3029.5 cm^{-1} were O–H bonds. The peak of 3477.6 cm^{-1} in the wires moved to 3425 cm^{-1} . The characteristic absorption peak of the hydroxyl group [7], which coordinated with the metal cations, moved from 1900–1650 to 1577.8 cm^{-1} [8]. Given the strong coupling effect, the characteristic absorption of FTIR was split into two peaks: an antisymmetric stretching vibration (1577.8 cm^{-1}) and a symmetric stretching vibration (1438.5 cm^{-1}). The strength of 1577.8 cm^{-1} was strong in the FTIR curve but weak in the Raman curve. The absorption bands between 1309.7 and 1076.3 cm^{-1} were the stretching vibration of C–O [9].

In the Raman curve, the peaks at 3477.6 and 3029.5 cm^{-1} were O–H bonds. A peak was observed at 3029.5 cm^{-1} in the precursor, but was weaker in the wires. The peak in the wires moved from 3425 to 3477.6 cm^{-1} and was wider than the precursor peak. This situation also occurred on the IR curves. The absorption bands located at 2948.5 and 1438.5 cm^{-1} were the stretching vibrations and in-plane bending vibrations of $-\text{CH}_2$ [7, 8], respectively. The vibronic coupling of multiple CH_2 caused the split peaks of 2948.5 cm^{-1} , which were weaker in the IR curve. The wave numbers at 969.5 and 834.6 cm^{-1} might be the rocking vibration of the $-\text{CH}_2$ bond. Relative strength was opposite in the two samples. The XRD test results showed the change in structure, and the slight changes in the FTIR and Raman curves proved that the groups in the precursor and the wires were different.

The heating rate was 10 K min^{-1} . The thermogravimetric curve (see Fig. 3) showed the loss of water molecules and the thermal decomposition of calcium citrate. In process I, 8.25 and 6.93% mass

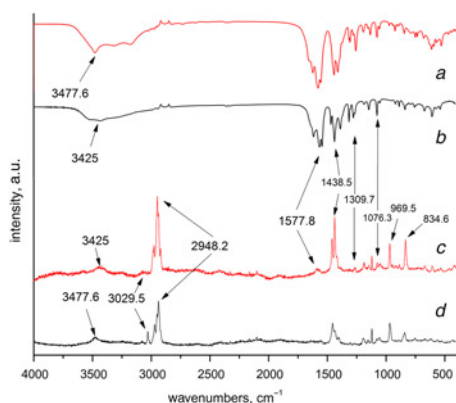


Figure 2 FTIR and Raman spectra of precursor and calcium citrate wires
a FTIR spectra of precursor; b FTIR spectra of wires; c Raman spectra of wires; d Raman spectra of precursor

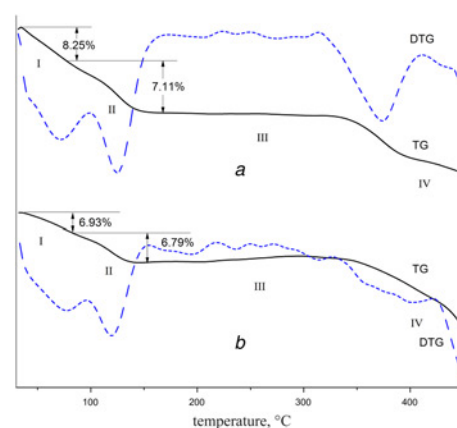


Figure 3 Thermogravimetric and derivative thermogravimetric curves of precursor and calcium citrate wires
a Wires
b Precursor

loss occurred at 50 and 76.9°C, respectively. Mansour [10] determined that mass loss resulted from the release of two water molecules from $\text{Ca}_3(\text{C}_6\text{H}_5\text{O}_7)_2 \cdot 4\text{H}_2\text{O}$. Mass loss was 6.3% in the theoretical calculation. The difference between the theoretical and actual measurements may be attributed to instrumental error and absorbed water. The mass loss of the wires was more than that of the precursor because the wire samples probably absorbed more water than the precursor.

In process II, 7.11 and 6.79% mass loss occurred at 77 and 120°C, respectively. $\text{Ca}_3(\text{C}_6\text{H}_5\text{O}_7)_2 \cdot 2\text{H}_2\text{O}$ transformed into $\text{Ca}_3(\text{C}_6\text{H}_5\text{O}_7)_2$ [9]. Mass loss was 6.74% in the theoretical calculation. The theoretical result agrees well with the experimental results.

The small mass-invariant curve of process III (120–350°C) could be attributed to the melting of calcium citrate, whereas that of process IV (over 350°C) was caused by calcium citrate that decomposed into CaCO_3 [10].

The SEM images (Figs. 4*a–e*) showed the morphology of calcium citrate that underwent different heating times at the same temperature. As shown in Fig. 4*a*, the precursor that was precipitated with alcohol was a sheet that measured $\sim 200\text{--}800\text{ nm} \times 100\text{--}400\text{ nm} \times 8\text{--}30\text{ nm}$.

Meanwhile, Figs. 4*b–e* show the process in which the precursor transformed into wires during heating in the alcohol–water mixture. The wire ratio increased with heating time. The precursor formed complete lamellas (Fig. 4*b*) and many lamellas remained when the heating time was 2 h (Fig. 4*b*); however, long wires were formed. The lamellas disappeared after 6 h (Fig. 4*d*), and the wires became uniform and narrow as heating time increased (8 h, Fig. 4*e*). The formation of wires proved that a preferred growth orientation occurred. The width of the wires was 50–200 nm, and their thickness was 8–30 nm. The wires are nearly consecutive in the images. These wires could be assumed as long wires.

In Fig. 4*b*, the long wires appear clear but many precursors remain. Tiny calcium citrate crystals formed and became seeds when the solution was heated because the solubility of calcium citrate decreased with temperature. A preferred orientation was required for seeds to grow into wires. The amount of sheet precursors was reduced with time, as shown in Figs. 4*b–e*.

These Figures reveal that the dissolution–reprecipitation mechanism was used in the process of growing wires. The precursor dissolved in the mixed solution, although most of it remained when heating started. Thereby, the remaining precursor continued to dissolve as the wires grew until it dissolved completely and turned into wires. The influence of alcohol could change the free energy and increase the supersaturation state of the mixture [11]. The change in interfacial energy between the solution and the crystal would

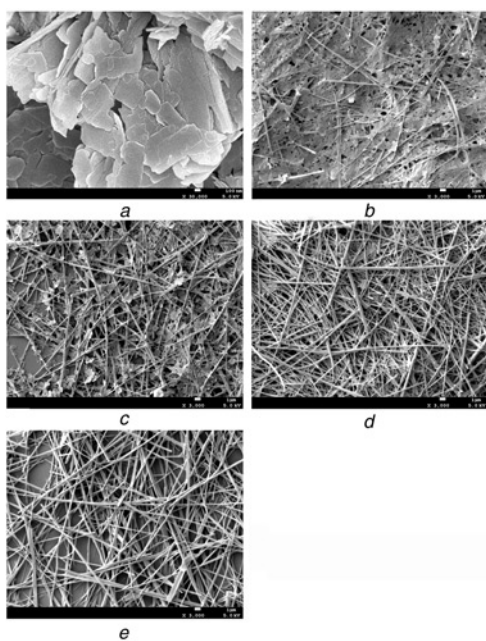


Figure 4 SEM images of precursor that underwent heating at different times

- a 0 h, alcohol–water mixture
- b 2 h, alcohol–water mixture
- c 4 h, alcohol–water mixture
- d 6 h, alcohol–water mixture
- e 8 h, alcohol–water mixture

promote the transformation of the sheet. Moreover, the alcohol could be adsorbed [12] to the crystal surface by forming a hydrogen bond between COO^- and OH^- . Different crystal planes were likely to adsorb varying amounts of alcohol, and thus, the ion concentration in the crystal planes was different and the growth velocity of the crystal planes would be different. The preferential crystal plane would appear when the growth velocity of one plane was normal but those of the others had slowed down [13]. The XRD test results indicated that (200) was the preferential crystal plane. Therefore further research is necessary.

4. Conclusion: Long wires were obtained by heating a sheet precursor in an alcohol–distilled water mixture in an open vessel. The precursor was precipitated from the mixed solution of calcium chloride and sodium citrate by adding alcohol. The wires formed were $\sim 50\text{--}300$ nm wide and $8\text{--}30$ nm thick. Moreover,

the wires were consecutive based on the SEM images, which also showed that a preferred orientation growth appeared as the wires grew. The XRD results indicated that the (200) plane was the most obvious preferential crystal plane. This result was attributed to the adsorption of alcohol, which could change the free energy and increase the supersaturation state of the mixture. The results of the FTIR and the thermal analysis showed that the amount of water molecules was different in the precursor and the wires. The structure and property might differ from those of calcium citrate produced using a traditional method. Novel applications of calcium citrate wires should be investigated in the future.

5 References

- [1] Huang S., Chen J.C., Hsu C.W., Chang W.H.: 'Effects of nano calcium carbonate and nano calcium citrate on toxicity in ICR mice and on bone mineral density in an ovariectomized mice model', *Nanotechnology*, 2009, **20**, (37), p. 375102
- [2] Zhang W., Wang W., Chen Q.Y., *ET AL.*: 'Effect of calcium citrate on bone integration in a rabbit femur defect model', *Asian Pac. J. Trop. Med.*, 2012, **5**, (4), pp. 310–314
- [3] Li-ming W., Wei W., Xiu-cui L., Lei P., Zhong-qin L., Hua-zi X.: 'Calcium citrate: a new biomaterial that can enhance bone formation in situ', *Asian Pac. J. Trop. Med.*, 2012, (5), pp. 291–296
- [4] Parsons A.J., Ahmed I., Haque P., *ET AL.*: 'Phosphate glass fibre composites for bone repair', *J. Bionic Eng.*, 2009, **6**, (4), pp. 318–323
- [5] Xing D.: 'The research of the biotype calcium citrate bone material and related studies'. Master thesis, Wenzhou Medical College, 2008
- [6] Herdtweck E., Kornprobst T., Sieber R., Straver L., Plank J.: 'Crystal structure, synthesis, and properties of tri-calcium di-citrate tetrahydrate $[\text{Ca}_3(\text{C}_6\text{H}_5\text{O}_7)_2(\text{H}_2\text{O})_2] \cdot 2\text{H}_2\text{O}$ ', *Z. Anorg. Allg. Chem.*, 2011, **637**, (6), pp. 655–659
- [7] Shriner R.L., Hermann C.K.F., Morrill T.C., Curtin D.Y., Fuson R. C.: 'The systematic identification of organic compounds' (John Wiley & Sons Inc, New York, NY, 2004, 8th edn)
- [8] Xiu-ming D., Lei P., Feng W.: 'Simulated body fluid immersion method for assessing biological characteristics of calcium citrate', *Chin. J. Tissue Eng. Res.*, 2013, **17**, (38), pp. 6811–6816
- [9] Dean J.A.: 'Lange's chemistry handbook version' (McGraw-Hill, 1999, 15th edn)
- [10] Mansour S.A.A.: 'Thermal decomposition of calcium citrate tetrahydrate', *Thermochimica Acta*, 1994, **233**, (2), pp. 243–256
- [11] Hacherl J.M., Paul E.L., Buettner H.M.: 'Investigation of impinging-jet crystallization with a calcium oxalate model system', *AIChE J.*, 2003, **49**, (9), pp. 2352–2362
- [12] Wu J., Xiao Y., Liang H., Feng Y.T., Zeng H.Z.: 'Butanol-frequency microwave-hydrothermal synthesis and characterization of high-quality hydrous magnesium oxysulfate whiskers', *J. Synth. Cryst.*, 2009, **38**, pp. 285–289
- [13] Zhang X., Luo H., Zhong W.: 'Growth units model of anion coordination-polyhedra and its application to crystal growth', *Sci. China Ser. E, Technol. Sci.*, 2004, **47**, (2), pp. 191–202